Dimensionality-enhanced quantum state transfer in long-range-interacting spin systems

Samihr Hermes,[1,*] Tony J. G. Apollaro,[2,†] Simone Paganelli,[3,‡] and Tommaso Macrì[1,4,§]

[1]*Departamento de Física Teórica e Experimental, Universidade Federal do Rio Grande do Norte, Natal-RN, Brazil*

[2]*Department of Physics, University of Malta, Msida MSD 2080, Malta*

[3]*Dipartimento di Scienze Fisiche e Chimiche, Università dell'Aquila, via Vetoio, I-67010 Coppito-L'Aquila, Italy*

[4]*International Institute of Physics, Natal-RN, Brazil*

(Received 18 December 2019; revised manuscript received 8 April 2020; accepted 13 April 2020; published 4 May 2020)

In this work we study the single-qubit quantum state transfer in uniform long-range spin XXZ systems in high-dimensional geometries. We consider prototypical long-range spin exchanges that are relevant for experiments in cold atomic platforms: Coulomb, dipolar, and van der Waals-like interactions. We find that in all these cases the fidelity increases with the dimensionality of the lattice. We also find a pronounced enhancement of the fidelity in one-dimensional lattices for increasing interaction range. This can be related to the emergence of a pair of bilocalized states on the sender and receiver site due to the onset of an effective weak-coupling Hamiltonian. Finally, we test our predictions in the presence of temperature-induced disorder introducing a model for the thermal displacement of the lattice sites, considered as a set of local adiabatic oscillators.

DOI: 10.1103/PhysRevA.101.053607

I. INTRODUCTION

Quantum information processing requires suitable transfer protocols for transmitting a quantum state between different parties. This task turns out to be nontrivial because of the decoherence induced by the unavoidable interaction with an environment. Quantum state transfer (QST) has been achieved over large distances by spatial transmission of the particle carrying the state (*flying qubit*) [1–4]. Photons are a natural choice for flying qubits, and this strategy has been successfully employed in cavity QED devices. Another option, also suitable for long-distance transmission, is creating an entangled state to be shared between the parties, sender and receiver, in order to implement a teleportation protocol [5,6].

However, photons are not always the ideal choice to implement scalable quantum architectures where an efficient short-distance transmission is requested, e.g., in solid-state-based quantum computers. Here a more desirable option would be exploiting the natural dynamics of some excitations carrying the quantum information encoded in its quantum state. The most widely investigated model to perform such a task is a spin-$\frac{1}{2}$ Hamiltonian, where the initial state is encoded into one or more spins, accessible to a sender, and it is retrieved, after a certain time, on an equivalent set of spins accessible to a receiver [7–10].

Different strategies have been proposed to optimize the QST fidelity: almost perfect state transfer can be obtained in time-independent uniform chains [11–13], by modulated interactions [8,14], in disordered chains [15,16], exploiting the ballistic regime of the excitations [8,17–21], in the regime of weakly coupled sender and receiver[11,12,20,22–25], creating nearly resonant edge states introducing strong magnetic fields [23,26,27] and by topological protection [28,29] (for more detailed reviews see Refs. [30,31]).

Many steps forward have been done, both concerning the QST of many-qubit systems [32–34] and in the implementation schemes ranging from optomechanical arrays [35] and quantum dots [36–39] to ultracold atoms [24,40].

Much effort has been put into accomplishing quantum computing hardware with atom traps [41–43], since these schemes can be easily mapped into a many-body spin-1/2 model. In this context, different systems, such as polar molecules, trapped ions, and Rydberg atoms, are characterized by long-range interactions, possibly mediated by long-wavelength modes such as cavity photons, decreasing with distance as a power law [44–51]. Here some of the results obtained for next nearest-neighbors interactions do not apply; in particular the estimation of the transmission time becomes more demanding because of the breakdown of the Lieb-Robinson bound [52]. QST has been studied for long-range-interacting systems [16,53–56] with high fidelity and time speedup.

In this paper we analyze different long-range spin models, and we show that when the quantum channel is made of a two- (three-) dimensional (2D or 3D, respectively) lattice with uniform coupling, it is possible to achieve larger fidelity with respect to the case of a one-dimensional (1D) channel with the same Hamiltonian parameters.

In Sec. II we define the spin model and review the basic features of QST in quantum spin chains with short- and long-range couplings. In Sec. III we discuss our results on QST with paradigmatic long-range spin exchange scaling as $1/r^{\alpha}$ ($\alpha > 0$) as the Coulomb interaction ($\alpha = 1$), dipolar ($\alpha = 3$), and van der Waals ($\alpha = 6$), as well as the case of

*hermes@fisica.ufrn.br
†tony.apollaro@um.edu.mt
‡simone.paganelli@univaq.it
§macri@fisica.ufrn.br

($\alpha = 1/2$) relevant for ion-trap experiments in 1D, 2D, and 3D geometries. In Sec. III A we analyze the effect of vacancies as a way to improve the QST in these models and interpret the results by looking at the spectrum of effective two-spin models. The relevance of symmetry in the removal of spins in the chain is emphasized. In Sec. III B we discuss finite temperature effects leading to a displacement of the spins with respect to their equilibrium position. Finally, in Sec. IV we present our conclusions and propose some extensions of our work.

II. QUANTUM STATE TRANSFER IN THE *XXZ* MODEL

We consider a long-range XXZ spin model with Hamiltonian

$$\hat{H} = \sum_{\substack{i,j=1 \\ i<j}}^{N} \frac{C}{2a^{\alpha}|\mathbf{r}_i - \mathbf{r}_j|^{\alpha}} \left(\hat{S}_i^{+}\hat{S}_j^{-} + \hat{S}_i^{-}\hat{S}_j^{+} + 2\Delta \hat{S}_i^{z}\hat{S}_j^{z}\right), \quad (1)$$

where $S^{\pm}$ and S^{z} are spin-1/2 operators. The couplings C and Δ denote the intensity of the spin-exchange interaction and the anisotropy parameter, whereas α is the power-law exponent of the long-range coupling, and a is the lattice spacing among nearest-neighbor spins in the lattice. For simplicity we set $C = 1$ in units of energy $\times\, a^{\alpha}$ throughout our work, while $\mathbf{r}_i$ are dimensionless positions of the spins in units of a. For $\Delta = 0$ one obtains the isotropic long-range XY model, for $\Delta = 1$ one recovers the isotropic long-range Heisenberg model, and for $\Delta = \infty$ we obtain the long-range (classical) Ising model. The nearest-neighbor ($\alpha = \infty$) isotropic Heisenberg model was first considered in the seminal paper by Bose [7]. See the Appendix for the generalization of these results to higher dimensions. In this work we vary the long-range exponent $\alpha > 0$ and set the anisotropy parameter $\Delta = -2$. We notice that for $\Delta = -2$ we can rewrite the spin couplings in the form of a dipolar exchange potential

$$\hat{H}_{dip} = \sum_{ij} J_{ij}\left(\hat{\mathbf{S}}_i \cdot \hat{\mathbf{S}}_j - 3\hat{S}_i^{z}\hat{S}_j^{z}\right), \quad (2)$$

where $J_{ij} = C/2a^{\alpha}|\mathbf{r}_i - \mathbf{r}_j|^{\alpha}$.

The protocol describing the dynamics of our setup is described in Fig. 1 for a 2D setup. The 1D and 3D setups will be explicitly discussed below. In Fig. 1(a) the system of N spin-1/2 is initialized in the ferromagnetic state $\otimes_i|\downarrow\rangle_i$ in the z basis. At $t = 0$ one spin, the sender (in orange) is placed into a state $|\psi_s\rangle = \cos\frac{\theta}{2}|\downarrow\rangle + e^{i\phi}\sin\frac{\theta}{2}|\uparrow\rangle$. Here $\theta \in [0, \pi]$ and $\phi \in [0, 2\pi]$ are the usual angles defining a single qubit state in the Bloch sphere. The system is then left to evolve under unitary dynamics with the Hamiltonian Eq. (1). Additional effects such as decoherence, excited state decay, or a generic coupling to an external reservoir will be considered elsewhere, while the effects of temperature-induced positional disorder will be thoroughly discussed in Sec. III B.

We observe that for the model we are considering the total magnetization is preserved, i.e., $[\hat{H}\sum_{i=1}^{N} S^{z}] = 0$. Therefore the Hilbert space where the dynamics takes place is confined to the zero-excitation sector consisting of the fully ferromagnetic state $\otimes_i|\downarrow\rangle^i$ and the one excitation sector consisting of N states, where $N-1$ spins are in the $|\downarrow\rangle$ configuration and one is in the $|\uparrow\rangle$ configuration. Under these conditions one can redefine the many-body states in the computational basis as

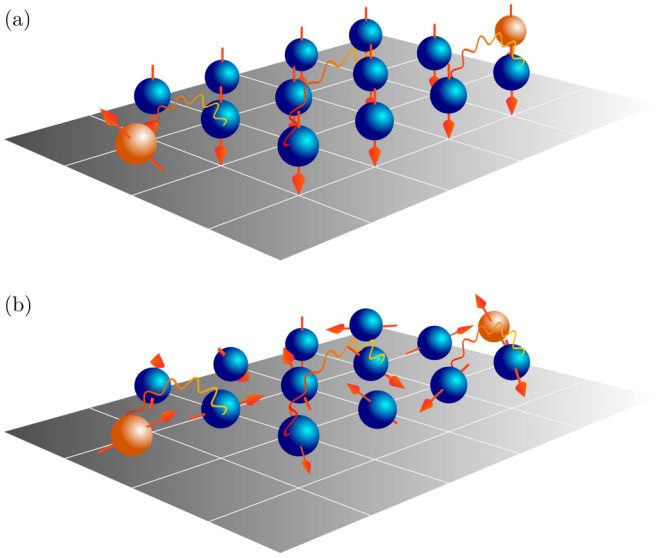

FIG. 1. Dynamical evolution of a quantum spin system with long-range interactions in a 2D array. Sender and receiver (orange) and the channel (blue) interact via a long-range spin-exchange interaction $1/r^{\alpha}$. At $t = 0$ the system is the state $|\psi_s\rangle = \alpha|0\rangle + \beta|1\rangle$ with one excitation localized at the sender $i = 1$. After a certain time t the state $|\psi_s\rangle$ of the sender can be found with high fidelity at the receiver $i = N$.

$$\otimes_i|\downarrow\rangle_i \equiv |\mathbf{0}\rangle, \quad (3)$$

$$|\uparrow\rangle_j \otimes_{i\neq j}|\downarrow\rangle_i \equiv |\mathbf{j}\rangle, \quad (4)$$

that belong to a subspace $\mathbf{H}$ of dimension $N+1$ of the full Hilbert space. For our calculations we perform exact numerical diagonalization of the Hamiltonian matrix of Eq. (1) in the basis above. Taking $\frac{C}{2a^{\alpha}} = 1$, we have the nontrivial diagonal and off-diagonal elements for $j \neq 0$:

$$\langle \mathbf{j}|\hat{H}|\mathbf{j}\rangle = \frac{\Delta}{2}\left(\sum_{\substack{k,l=1 \\ k<l}}^{N} \frac{1}{|\mathbf{r}_k - \mathbf{r}_l|^{\alpha}} - 2\sum_{\substack{i=1 \\ i\neq j}}^{N} \frac{1}{|\mathbf{r}_i - \mathbf{r}_j|^{\alpha}}\right), \quad (5)$$

$$\langle \mathbf{i}|\hat{H}|\mathbf{j}\rangle = \frac{1}{|\mathbf{r}_i - \mathbf{r}_j|^{\alpha}}. \quad (6)$$

For the special case of nearest-neighbor exchange interactions one has

$$\langle \mathbf{i}|\hat{H}|\mathbf{j}\rangle = \begin{cases} 0 & \text{if} \quad |\mathbf{r}_i - \mathbf{r}_j| \neq 1 \\ 1 & \text{otherwise} \end{cases},$$

$$\langle \mathbf{j}|\hat{H}|\mathbf{j}\rangle = \sum_{\substack{i,k=1 \\ i<k}}^{N} S_{ik},$$

where

$$S_{ik} = \begin{cases} \frac{\Delta}{2} \text{ if } |\mathbf{r}_i - \mathbf{r}_k| = 1 \text{ and } j \neq i,k, \\ -\frac{\Delta}{2} \text{ if } |\mathbf{r}_i - \mathbf{r}_k| = 1 \text{ and } j = i \text{ or } j = k, \\ 0 \text{ otherwise.} \end{cases} \quad (7)$$

The receiver's state at time t is given by $\rho_r(t) = \mathrm{Tr}_{\neg r}[|\Psi(t)\rangle\langle\Psi(t)|]$, where the trace is over all spins but the receiver. Hence, the fidelity between the receiver and a given sender state is given by $F(|\psi_s\rangle, t) = \langle\psi_s|\rho_r(t)|\psi_s\rangle$. However, as the initial state of the sender is generally unknown—otherwise it could be transferred with unit fidelity by LOCC—generally the average fidelity $F(t)$ is used as a figure of merit of the quality of a QST protocol from the sender to the receiver (orange spins in Fig. 1). $F(t)$ is readily obtained from $F(|\psi_s\rangle, t)$ by integrating over all possible pure input states on the Bloch sphere [16],

$$F(t) = \int \frac{d\Omega}{4\pi} \langle\psi_s|\rho_r(t)|\psi_s\rangle. \tag{8}$$

Upon integration we obtain the general expression

$$F(t) = \tfrac{1}{6}|f_{r,s}(t)|^2 + \tfrac{1}{3}|f_{r,s}(t)|\cos\gamma + \tfrac{1}{2}, \tag{9}$$

where we defined $f_{r,s}(t) = \langle\mathbf{r}|e^{-i\hat{H}t}|\mathbf{s}\rangle$, $\cos\gamma = \arg\{f_{r,s}(t)\}$, and set $\hbar = 1$. $|\mathbf{s}\rangle$ and $|\mathbf{r}\rangle$ are the singly excited states localized at the sender and receiver, respectively. In the following, we set in $F(t)$ the term $\cos\gamma = 1$, which is obtained by applying a magnetic field on the receiver state at the end of the QST [57]. Let us also mention that the presence of a uniform transverse magnetic field, $h\sum_{i=1}^{N}\hat{S}_i^z$, in Eq. (1) does not modify the fidelity because, in the single-particle sector, it corresponds to adding to Eq. (1) a term proportional to the identity. As a consequence, the eigenvectors remain unchanged and the single-particle eigenvalues experience a uniform shift yielding an overall irrelevant phase factor. Indeed, a uniform magnetic field can also be chosen [7] in such a way that $\cos\gamma = 1$.

In the next section we analyze the dynamics of $F(t)$ for configurations in one, two, and three dimensions as a function of the power-law exponent α.

III. QUANTUM STATE TRANSFER WITH LONG-RANGE COUPLINGS

In this section we discuss the maximum fidelity achievable for the QST in a long-range-interacting system in one, two, and three dimensions for different power-law interaction potentials. In Fig. 2 we show the results of the simulations. In the 1D configuration (red dots) sender and receiver are located at the extremes of the chain. In two dimensions (blue squares) we consider a rectangle lattice with $L \times 5$ spins where sender and receiver are placed as in Fig. 1. In three dimensions (gray diamonds) we examine a cubic lattice with $(L \times 5 \times 5)$ spins where sender and receiver are located next to the center of two opposite faces of the parallelepiped with 5×5 spins, at the distance a from the central spin. The exponents of the power-law interaction that we analyze are Fig. 1(a) $\alpha = 0.5$, Fig. 1(b) $\alpha = 1$, Fig. 1(c) $\alpha = 3$, and Fig. 1(d) $\alpha = 6$. We notice that the higher the dimensionality of the lattice, the higher is the fidelity. Furthermore, the enhancement is more pronounced the larger the system, and in 3D lattices the fidelity even stays close to one for relatively large system sizes.

From Fig. 2 we notice that, especially for 1D systems, the fidelity increases with the range of the interaction. Furthermore, for fixed α, the higher the dimensionality of the lattice the higher the fidelity. One can relate the interaction-range and dimensionality enhancement of the fidelity to an effective

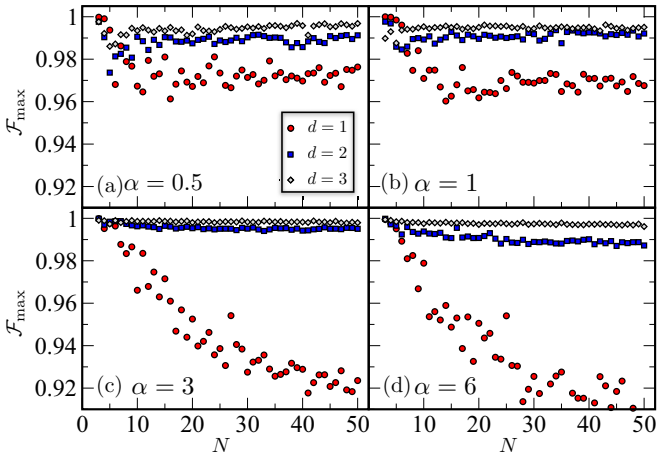

FIG. 2. Maximum fidelity for quantum state transfer in a long-range-interacting system in one, two, and three dimensions for different power-law interaction potentials and $\Delta = -2$. Red dot: $d = 1$, blue square: $d = 2$, gray diamond: $d = 3$. L is the linear size of the system. In two (three) dimensions we consider a rectangle (parallelepiped) lattice with $L \times 5$ ($L \times 5 \times 5$) spins. In two dimensions the sender and the receiver are located as in Fig. 1. In three dimensions they are located in the center of the square section of opposite faces of the parallelepiped, at distance a from the central spin. The exponent of the power-law interaction is (a) $\alpha = 0.5$, (b) $\alpha = 1$, (c) $\alpha = 3$, and (d) $\alpha = 6$. Fidelity increases with the dimensionality of the system for each power-law interaction. We notice that in three dimensions the fidelity stays close to one even for a large system size. The maximum fidelity is obtained by following the dynamics in the interval $t \in [0, t_{\Delta E}]$ The time $t_{\Delta E} \approx \hbar/\Delta E$ is estimated to be inversely proportional to the difference ΔE of the two eigenvalues with largest overlap with the sender and the receiver.

weak-coupling effect. To illustrate this effect in a qualitative way, let us first consider the interaction-range enhancement. From Eqs. (5) and (6) we notice that all k diagonals of the matrix representing the Hamiltonian in direct space are constant, but for $k = 0$. This is a consequence of the open boundary conditions. Whereas $k \neq 0$ secondary diagonals are given by Eq. (6) implying a constant term along the kth diagonal for fixed $k = i - j$, the terms in Eq. (5) depend on the position j. As a consequence, for $k = 0$ (the main diagonal), $\langle\mathbf{j}|\hat{H}|\mathbf{j}\rangle$ decreases, due to the second term in the RHS, for j closer to the edges; see, e.g., Fig. 5 of Ref. [53]. This embodies the boundary effect that spins closer to the edges have less spins at shorter distances $|\mathbf{r_i} - \mathbf{r_j}|$ than spins located more towards the center of the system. Clearly, at fixed α, this boundary effect is enhanced with the dimensionality of the system.

As a consequence, the dynamics of the model in Eq. (1), when restricted to the single-particle sector, is equivalent to that of an Hamiltonian where the last term of Eq. (1) is replaced by an effective magnetic field acting on site j with intensity along the z direction given by Eq. (5). The aforementioned effective magnetic field on the sender and receiver spins weak with respect to that on the spins located in the quantum channel, the QST mechanism is equivalent to that falling into the class of the weak-coupling regime

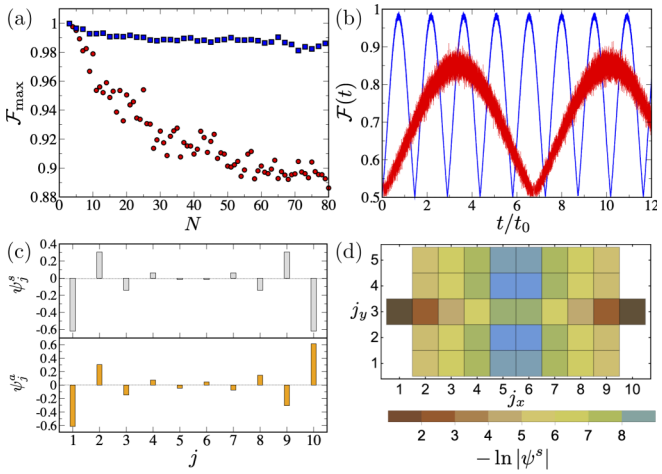

FIG. 3. Quantum state transfer for a long-range-interacting 1D and 2D system with $\alpha = 6$ (van der Walls interactions) and $\Delta = -2$ of the XXZ model of Eq. (1). a) Maximum value of the fidelity for a system with N spins ($N = 2, \ldots, 100$). Red dots: 1D chain with N spins. Blue squares: 2D $L \times 5$ setup as in (d). (b) Dynamical evolution of the fidelity as a function of the rescaled time t/t_0. The time $t_0 = \pi a^\alpha (L-1)^\alpha / C\hbar^2$ is the time it takes for the two-spin system (sender and receiver) to perform an ideal quantum state transfer for $N = 50$. (c) Symmetric and antisymmetric eigenstates $\psi^{(s,a)}$ with the greatest overlap with the sender and the receiver, which are responsible for the high-fidelity state transfer for the 1D case. (d) Overlap of the bilocalized states with the sender and the receiver for a 2D system with 10×5 (the number of spins in the line containing the sender and receiver is $L = 10$, and the height 5). Notice that, as the the overlap is plotted in the natural logarithmic scale, the figure is identical for the symmetric and antisymmetric state.

QST protocols [11,26,27]. These protocols are characterized by the presence of a pair of quasidegenerate energy eigenstates, each bilocalized on the sender and receiver site, i.e., $|E^\pm\rangle = \sum_{i=1}^{N} \langle i|E^\pm\rangle |i\rangle \simeq a(|s\rangle \pm |r\rangle)$, reducing the dynamics to an effective two-level system bringing along Rabi-like oscillations of the excitation between the two locations. The more pronounced the overlap of these energy eigenstates with the sender and receiver site, with $a = \frac{1}{\sqrt{2}}$ representing perfect bilocalization, the higher the fidelity of the QST protocol. Notice that the appearance in the energy spectrum of a pair of quasidegenerate states, bilocalized on the sender and receiver sites, is witnessing an effective decoupling mechanism by which the sender and receiver site form an almost invariant subspace trapping the excitation on the two sites. A rigorous derivation of the equivalence of weak (strong) local magnetic fields and weak coupling is presented in Ref. [27] by means of perturbation theory.

A. Quantum state transfer in the presence of vacancies and the role of symmetry

In Fig. 3(a) we plot the maximum value of the fidelity for a system with N spins ($N = 2, \ldots, 100$) with the 1D chain (red dots) and 2D lattice with 10×5 spins (blue squares). In Fig. 3(b) we show the dynamical evolution of the fidelity as a function of the rescaled time t/t_0, where we define

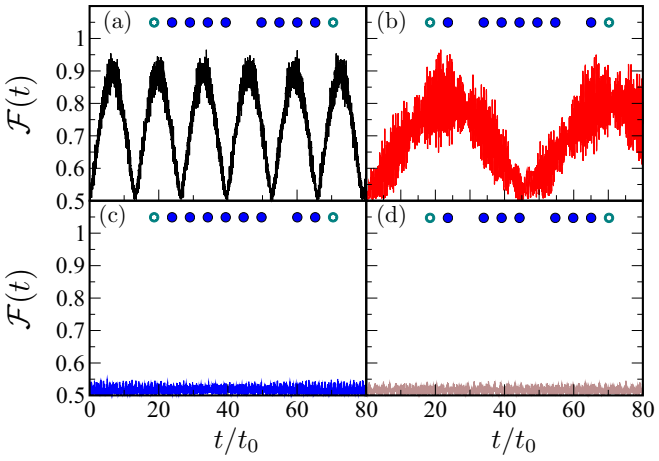

FIG. 4. Quantum state transfer and mirror symmetry of the vacancies in a linear chain with $\alpha = 1$. Dynamical evolution of the fidelity $\mathcal{F}(t)$ with one vacancy (a) and (c), and two vacancies (b) and (d). In (a) and (b) spins are removed symmetrically with respect to the center of the chain. In (c) and (d) vacancies are created randomly along the chain.

$t_0 = \pi a^\alpha (N-1)^\alpha / C\hbar^2$. t_0 is the time it takes for the two-spin system (sender and receiver) to perform an ideal quantum state transfer in the absence of the channel. As we discussed above, a quantitative explanation of the increase of the fidelity can be obtained by studying the eigenstates with maximal overlap with the sender and the receiver. In Figs. 3(c)–3(d) we plot the symmetric and antisymmetric eigenstates $\psi^{(s,a)}$, which are responsible for the state transfer for the regular chain with N spins (c) and for the 2D lattice 10×5 (d).

The Hamiltonian we consider in our work is mirror symmetric, which in Refs. [8,10] was found to be a necessary condition for perfect QST. Here we investigate the breaking of the mirror symmetry by removing arbitrary spins in the configurations. For simplicity we focus on 1D and 2D systems. The results are reported in Fig. 4 and Fig. 5.

In Fig. 4 we plot the configuration and the dynamics of the QST fidelity in a linear chain with Coulomb interaction

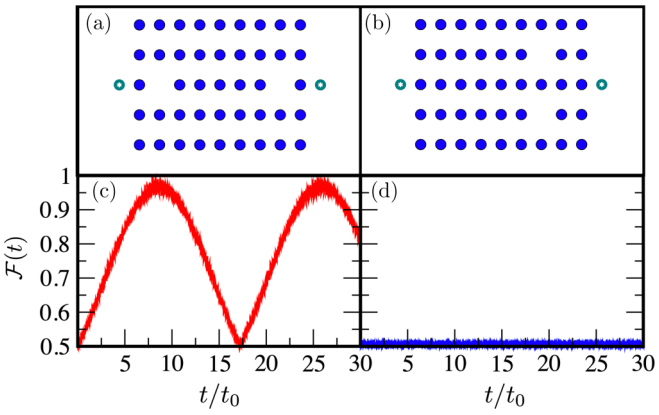

FIG. 5. Quantum state transfer and mirror symmetry of the vacancies in a 2D square lattice with $\alpha = 1$. Dynamical evolution of the fidelity $\mathcal{F}(t)$ with (a) two symmetric vacancies and (c) two asymmetric vacancies.

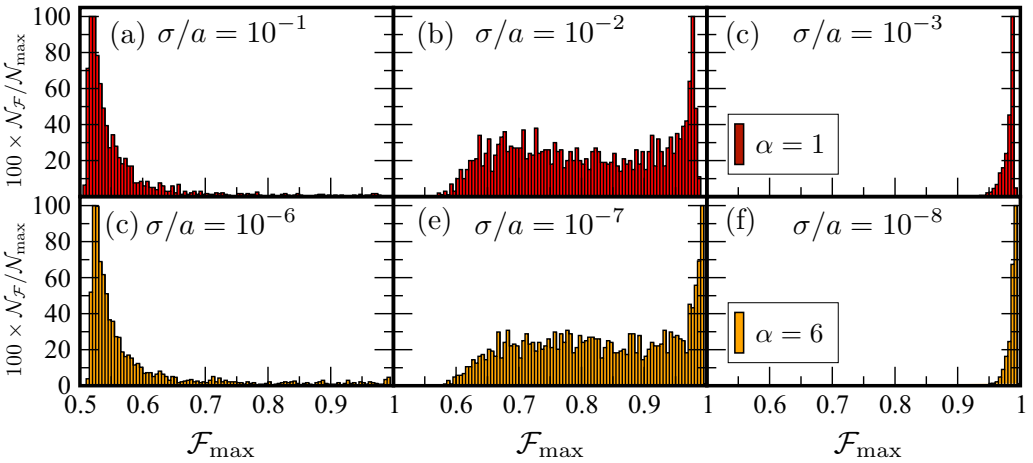

FIG. 6. Distribution of the maxima of the fidelities for Gaussian disordered atomic position configurations for several values of the disorder strength. Particles are displaced with respect to their equilibrium value according to a Gaussian distribution with width σ/a in a 2D lattice with length $L = 10$ and height $h = 4$. The strength of the disorder is connected to the temperature of the configuration as explained in the text. We consider $N_r = 2000$ realizations. (a–c) $\alpha = 1$ Coulomb spin-exchange interaction. (d–f) $\alpha = 6$ van der Walls spin-exchange interaction. The distribution of frequencies N_F is normalized to the peak value of each histogram $N_{\max}$.

$\alpha = 1$ in the presence of one and two vacancies. In Figs. 4(a) and 4(b) spins are removed symmetrically with respect to the center of the chain. In Figs. 4(c) and 4(d) vacancies are created randomly along the chain. Without mirror symmetry the fidelity decreases to approximately the random guess value of $\frac{1}{2}$. This corresponds to a vanishing probability for the excitation to reach the sender site; see Eq. (9). However, in the presence of mirror symmetry, the fidelity has maxima close to 1.

We repeat the analysis for a 2D system with a channel with 9×5 spins. We observe that, preserving mirror symmetry as in Figs. 5(a) and 5(b), the dynamics displays a high value of the fidelity. In contrast, when mirror symmetry is broken by the removal of two spins, fidelity decreases again to around $\frac{1}{2}$.

B. Finite temperature effects

We now discuss the effect of disorder in the particle configuration. We focus on the 2D case. However, the results can be generalized to both one and three dimensions straightforwardly. The motivation for this analysis is related to recent experiments on Rydberg atoms trapped in optical tweezers [58]. There atoms are trapped in a strongly focused laser field, with a small but finite dispersion of the position. We model this effect as a temperature-induced quenched disorder on the particle configuration as in Ref. [59]. This description is valid if the dynamics of the spin is decoupled from the motional degrees of freedom, i.e., if the time t_{id} associated to the QST protocol is much faster than the typical motional timescales $\hbar/k_B T$, where T is the temperature of the system. Then we model the dynamics of the motional degrees of freedom of particle i centered in the lattice site with coordinates (x_i^0, y_i^0) with a classical Boltzmann distribution $f(\mathbf{r}, \mathbf{p}) = \exp[-\beta H_m(\mathbf{r}, \mathbf{p})]$, where

$$H_m^{(i)}(\mathbf{r}, \mathbf{p}) = \sum_{j=x,y} \frac{p_j^2}{2m} + \frac{m}{2}\omega_j^2 (r_j - r_j^0)^2. \tag{10}$$

To find the distribution of the position $\bar{f}(x, y)$, we integrate the momentum contribution and normalize

$$\bar{f}(x, y) = \frac{1}{2\pi}\frac{1}{\sigma_x \sigma_y} \exp\left[-\frac{(x - \bar{x})^2}{2\sigma_x^2} - \frac{(y - \bar{y})^2}{2\sigma_y^2}\right], \tag{11}$$

where we defined the variance $\sigma_i^2 = 1/(\beta m \omega_i^2)$. We notice that, although we restrict our analysis to fluctuations along the plane x-y, if we were to fully model an experimental setup, the confinement along the z direction also should be considered. Therefore our study corresponds to the limiting case of vanishing σ_z. For simplicity, we are restricting it to $\sigma_x = \sigma_y = \sigma$. We observe that, although particle positions in the lattice are uncorrelated, interparticle distances (in the definition of the spin exchange couplings J_{ij}) are correlated [60].

The results of the simulations are shown in Fig. 6. We plot the distribution of the maxima of the fidelities for Gaussian disordered atomic position configurations for several values of the disorder strength σ/a rescaled to the lattice spacing. Particles are displaced with respect to their equilibrium value in a 2D lattice with length $L = 10$ and height $h = 4$. We consider $N_r = 2000$ realizations of the disorder and $\alpha = 1$ Coulomb spin-exchange interaction [Figs. 6(a)–6(c)] and $\alpha = 6$ van der Walls spin-exchange interaction ([Figs. 6(d)–6(f)]. For clarity the distribution is normalized to the peak value of each histogram. Fixing α and for low disorder the distribution is peaked close to unitary fidelities. Increasing the disorder strength a plateau appears in the distribution with a peak at $F_{\max} = 1$. By further increasing the disorder the distribution has a peak at $F_{\max} = 1/2$ and the plateau disappears. We notice that this behavior is quite generic for the long-range exponents that we analysed. The second relevant feature of the fidelity distributions is that, upon increasing α, smaller values of the disorder σ/a are needed to obtain a distribution peaked at higher fidelities. The qualitative explanation is that a longer-range interaction makes the system more insensitive to the fluctuation of particle positions. To be more quantitative, this

can be seen by computing the variation of the spin-exchange couplings as a function of the disorder [61]

$$\frac{\Delta J_{ij}}{J_{ij}} = \frac{\tilde{J}_{ij} - J_{ij}}{J_{ij}} = \frac{r_{ij}{}^{\alpha}}{|\mathbf{r}_{ij} + \delta|^{\alpha}} - 1, \tag{12}$$

where we defined $\mathbf{r}_{ij} = \mathbf{r}_i - \mathbf{r}_j$, $\tilde{J}_{ij} = C/2a^{\alpha}|\mathbf{r}_{ij} + \delta|^{\alpha}$, and δ is the difference of the fluctuations of the two particles. Monitoring the variation of $\frac{\Delta J_{ij}}{J_{ij}}$ as a function of α for a fixed equilibrium interparticle spacing and disorder strength, the ratio vanishes for $\alpha = 0$. This corresponds to a position-independent spin coupling that clearly should not depend on the specific value of disorder. In the opposite limit, when α increases the ratio $\frac{\Delta J_{ij}}{J_{ij}}$ decreases to the limiting value -1 for infinite α (position-dependent nearest-neighbor interaction). In this limit disorder dominates and the regularity of the particle configuration, including a strong breaking of mirror symmetry, leads to a dramatic reduction of the fidelity of the quantum state transfer.

IV. CONCLUSIONS

In this work we studied the problem of quantum state transfer in lattices with open boundary conditions in one, two, and three dimensions for the anisotropic Heisenberg XXZ model with of power-law couplings with variable exponent α and with a sender and receiver spin symmetrically coupled to its edges.

We first analyzed the case of regular lattices and found that the fidelity increases upon increasing the dimensionality of the lattice for sufficiently large system sizes, and the enhancement of the fidelity is more pronounced for systems with long-range interaction. We interpreted this result as a combined effect of the open boundaries of the lattice and the presence of the interspin interaction term in the z direction, resulting in an effective weak-coupling Hamiltonian in the single-excitation sector, although the couplings are all uniform. We justified this interpretation by noticing that the quantum state transfer takes place via Rabi-like oscillations involving only two single-particle eigenstates localized on the sender and receiver site, a mechanism that is related to resonant tunneling in effective decoupled models.

We studied also the effect of vacancies both in 1D and 2D lattices, confirming the necessity of the presence of mirror symmetry in the lattice configuration with the removed spins in order to increase the fidelity of the quantum transfer transfer. Also, for the relevant case of 1D systems, we observed that for longer-range interactions, one might consider a larger number of vacancies to obtain a higher fidelity. Finally, inspired by experiments of cold atoms in optical tweezers, we considered the effect of a finite temperature inducing displacements of the particles by studying the distribution of the maxima of the fidelity. We observed that, as a general property, longer range interactions suffer less from temperature-induced disorder than shorter range potentials. Quantitatively, this effect can be understood by analyzing the fluctuations of the spin couplings J_{ij} due to disorder as a function of the exponent α.

Our study is relevant for the characterization of quantum state transfer in experimental platforms for quantum simulation and technology. We were mostly inspired by applications to ultracold ions and atoms where long-range interactions are an intrinsic tool in the realization of spin models, e.g., in cold atoms trapped in a photonic crystal waveguide. Extensions of this work include the study of the effect of decoherence and excited state decay, relevant for experimental platforms. Calculations for open systems will be considered elsewhere.

ACKNOWLEDGMENTS

S.H. acknowledges CNPq for financial support. T.M. acknowledges CNPq for support through Bolsa de produtividade em Pesquisa no. 311079/2015-6. This work was supported by the Serrapilheira Institute (Grant no. Serra-1812-27802), CAPES-NUFFIC Project no. 88887.156521/2017-00. T.M. thanks the Physics Department of the University of L'Aquila for the hospitality where part of the work was done. The authors acknowledge S. M. Giampaolo for useful discussions.

APPENDIX: NEAREST-NEIGHBOR INTERACTIONS IN HIGHER LATTICES

In this Appendix we present the results of the maximum fidelity for nearest-neighbor interactions in a slab with linear dimension L and transverse length $L_{\perp} = 5$ in two dimensions and a parallelepiped $L_{\perp} \times L_{\perp} = 5 \times 5$ in three dimensions (Fig. 7). For a purely 1D system, our results are equivalent to Ref. [7] We observe that, similarly to the long-range case, fidelity is higher for a higher dimensional slab. However, the maximum fidelity is notably smaller than unity even for the 3D case, in contrast to Fig. 2, where for each $\alpha \leqslant 6$ fidelity is close to one even for very large sizes.

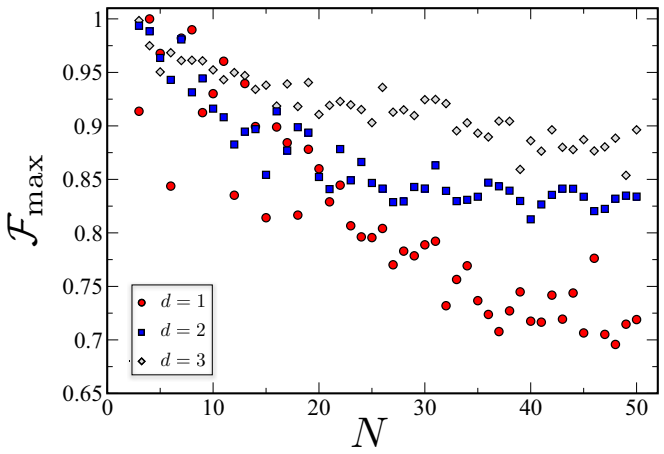

FIG. 7. Maximum fidelity for quantum state transfer in a nearest-neighbor interacting system in a 1D, 2D, and 3D slab and $\Delta = 1$ (isotropic Heisenberg model). Red dot: $d = 1$, blue square: $d = 2$, gray diamond: $d = 3$. N is the linear size of the system. In two (three) dimensions we consider a square (cubic) lattice with $N \times 5$ ($N \times 5 \times 5$) spins. In two dimensions the sender and the receiver are located as in Fig. 1. In three dimensions they are located in the center of two opposite faces of the cube, at distance a from the central spin. Fidelity increases with the the dimensionality of the system for sufficiently large system sizes.

[1] T. E. Northup and R. Blatt, Nat. Photon. **8**, 356 (2014).
[2] L.-M. Duan, M. D. Lukin, J. I. Cirac, and P. Zoller, Nature (London) **414**, 413 (2001).
[3] S. Ritter, C. Nölleke, C. Hahn, A. Reiserer, A. Neuzner, M. Uphoff, M. Mücke, E. Figueroa, J. Bochmann, and G. Rempe, Nature (London) **484**, 195 (2012).
[4] P. Kurpiers, P. Magnard, T. Walter, B. Royer, M. Pechal, J. Heinsoo, Y. Salathé, A. Akin, S. Storz, J.-C. Besse *et al.*, Nature (London) **558**, 264 (2018).
[5] C. H. Bennett, G. Brassard, C. Crépeau, R. Jozsa, A. Peres, and W. K. Wootters, Phys. Rev. Lett. **70**, 1895 (1993).
[6] X.-S. Ma, T. Herbst, T. Scheidl, D. Wang, S. Kropatschek, W. Naylor, B. Wittmann, A. Mech, J. Kofler, E. Anisimova *et al.*, Nature (London) **489**, 269 (2012).
[7] S. Bose, Phys. Rev. Lett. **91**, 207901 (2003).
[8] M. Christandl, N. Datta, A. Ekert, and A. Landahl, Phys. Rev. Lett. **92**, 187902 (2004).
[9] D. Burgarth and S. Bose, Phys. Rev. A **71**, 052315 (2005).
[10] M. Christandl, N. Datta, T. C. Dorlas, A. Ekert, A. J. Kay, and A. Landahl, Phys. Rev. A **71**, 032312 (2005).
[11] A. Wójcik, T. Łuczak, P. Kurzyński, A. Grudka, T. Gdala, and M. Bednarska, Phys. Rev. A **72**, 034303 (2005).
[12] L. Campos Venuti, C. Degli Esposti Boschi, and M. Roncaglia, Phys. Rev. Lett. **99**, 060401 (2007).
[13] L. Banchi, T. J. G. Apollaro, a. Cuccoli, R. Vaia, and P. Verrucchi, New J. Phys. **13**, 123006 (2011).
[14] K. Eckert, O. Romero-Isart, and A. Sanpera, New J. Phys. **9**, 155 (2007).
[15] D. Burgarth and S. Bose, New J. Phys. **7**, 135 (2005).
[16] G. M. Almeida, F. A. de Moura, and M. L. Lyra, Phys. Lett. A **382**, 1335 (2018).
[17] T. Osborne and N. Linden, Phys. Rev. A **69**, 052315 (2004).
[18] C. Di Franco, M. Paternostro, and M. S. Kim, Phys. Rev. Lett. **101**, 230502 (2008).
[19] C. Di Franco, M. Paternostro, and G. M. Palma, Int. J. Quantum Inf. **06**, 659 (2008).
[20] S. Paganelli, F. de Pasquale, and G. Giorgi, Phys. Rev. A **74**, 012316 (2006).
[21] L. Banchi, T. J. G. Apollaro, A. Cuccoli, R. Vaia, and P. Verrucchi, Phys. Rev. A **82**, 052321 (2010).
[22] M. B. Plenio and F. L. Semião, New J. Phys. **7**, 73 (2005).
[23] S. Paganelli, S. Lorenzo, T. J. G. Apollaro, F. Plastina, and G. L. Giorgi, Phys. Rev. A **87**, 062309 (2013).
[24] S. Lorenzo, T. J. G. Apollaro, A. Trombettoni, and S. Paganelli, Int. J. Quantum Inf. **15**, 1750037 (2017).
[25] W. J. Chetcuti, C. Sanavio, S. Lorenzo, and T. J. G. Apollaro, New J. Phys. **22**, 033030 (2020).
[26] F. Plastina and T. J. G. Apollaro, Phys. Rev. Lett. **99**, 177210 (2007).
[27] S. Lorenzo, T. J. G. Apollaro, A. Sindona, and F. Plastina, Phys. Rev. A **87**, 042313 (2013).
[28] F. Mei, G. Chen, L. Tian, S.-L. Zhu, and S. Jia, Phys. Rev. A **98**, 012331 (2018).
[29] S. Longhi, G. L. Giorgi, and R. Zambrini, Advanced Quantum Technologies **2**, 1800090 (2019).
[30] S. Bose, Contemp. Phys. **48**, 13 (2007).
[31] T. J. G. Apollaro, S. Lorenzo, and F. Plastina, Int. J. Mod. Phys. B **27**, 1345035 (2013).
[32] S. Lorenzo, T. J. G. Apollaro, S. Paganelli, G. M. Palma, and F. Plastina, Phys. Rev. A **91**, 042321 (2015).
[33] R. Sousa and Y. Omar, New J. Phys. **16**, 123003 (2014).
[34] T. J. G. Apollaro, S. Lorenzo, A. Sindona, S. Paganelli, G. L. Giorgi, and F. Plastina, Physica Scripta **T165**, 014036 (2015).
[35] G. D. de Moraes Neto, F. M. Andrade, V. Montenegro, and S. Bose, Phys. Rev. A **93**, 062339 (2016).
[36] U. Farooq, A. Bayat, S. Mancini, and S. Bose, Phys. Rev. B **91**, 134303 (2015).
[37] B. E. Kane, Nature (London) **393**, 133 (1998).
[38] D. Loss and D. P. DiVincenzo, Phys. Rev. A **57**, 120 (1998).
[39] F. de Pasquale, G. L. Giorgi, and S. Paganelli, Phys. Rev. A **71**, 042304 (2005).
[40] A. G. Volosniev, D. Petrosyan, M. Valiente, D. V. Fedorov, A. S. Jensen, and N. T. Zinner, Phys. Rev. A **91**, 023620 (2015).
[41] R. Vrijen and E. Yablonovitch, Physica E **10**, 569 (2001).
[42] D. Kielpinski, C. Monroe, and D. J. Wineland, Nature (London) **417**, 709 (2002).
[43] M. Saffman, J. Phys. B **49**, (2016).
[44] B. Gadway and B. Yan, J. Phys. B **49**, 152002 (2016).
[45] T. Lahaye, C. Menotti, L. Santos, M. Lewenstein, and T. Pfau, Rep. Prog. Phys. **72**, 126401 (2009).
[46] D. Leibfried, R. Blatt, C. Monroe, and D. Wineland, Rev. Mod. Phys. **75**, 281 (2003).
[47] C. D. Bruzewicz, J. Chiaverini, R. McConnell, and J. M. Sage, Appl. Phys. Rev. **6**, 021314 (2019).
[48] A. Browaeys, D. Barredo, and T. Lahaye, J. Phys. B **49**, 152001 (2016).
[49] H. Zhou, J. Choi, S. Choi, R. Landig, A. M. Douglas, J. Isoya, F. Jelezko, S. Onoda, H. Sumiya, P. Cappellaro *et al.*, arXiv:1907.10066 (2019).
[50] P. Schauß, J. Zeiher, T. Fukuhara, S. Hild, M. Cheneau, T. Macrì, T. Pohl, I. Bloch, and C. Gross, Science **347**, 1455 (2015).
[51] J. Zeiher, P. Schauß, S. Hild, T. Macrì, I. Bloch, and C. Gross, Phys. Rev. X **5**, 031015 (2015).
[52] E. H. Lieb and D. W. Robinson, Commun. Math. Phys **28**, 251 (1972).
[53] G. Gualdi, V. Kostak, I. Marzoli, and P. Tombesi, Phys. Rev. A **78**, 022325 (2008).
[54] M. Avellino, A. J. Fisher, and S. Bose, Phys. Rev. A **74**, 012321 (2006).
[55] Z. Eldredge, Z.-X. Gong, J. T. Young, A. H. Moosavian, M. Foss-Feig, and A. V. Gorshkov, Phys. Rev. Lett. **119**, 170503 (2017).
[56] N. Y. Yao, L. Jiang, A. V. Gorshkov, Z.-X. Gong, A. Zhai, L.-M. Duan, and M. D. Lukin, Phys. Rev. Lett. **106**, 040505 (2011).
[57] A. Zwick, G. A. Álvarez, J. Stolze, and O. Osenda, Quantum Inf. Comput. **15**, 582 (2015).
[58] H. Labuhn, D. Barredo, S. Ravets, S. de Léséleuc, T. Macrì, T. Lahaye, and A. Browaeys, Nature (London) **534**, 667 (2016).
[59] D. Barredo, V. Lienhard, S. de Léséleuc, T. Lahaye, and A. Browaeys, Nature (London) **561**, 79 (2017).
[60] M. Marcuzzi, J. Minář, D. Barredo, S. de Léséleuc, H. Labuhn, T. Lahaye, A. Browaeys, E. Levi, and I. Lesanovsky, Phys. Rev. Lett. **118**, 063606 (2017).
[61] R. Menu and T. Roscilde, Phys. Rev. Lett. **124**, 130604 (2020).